International Journal of Fracture 30 (1986) 301–315

Some evaluations of the elastic *T*-term using Eshelby's method

A.P. KFOURI

Department of Mechanical Engineering, University of Sheffield, Sheffield S1 3JD, England

(Received 24 May 1985; in revised form 15 October 1985)

Abstract

For some time now the elastic *T*-term has been proposed as a secondary "biaxiality" parameter, to be used in conjunction with the stress intensity factor, K_I, or the path independent integral J, as the primary parameter for the characterization of crack tip fracture states. At a recent conference a theorem due to Eshelby was presented [1]. The theorem provides a convenient method of calculating the *T*-term, obtained by evaluating appropriate J contour integrals. Examples of analytical, semi-analytical and numerical applications were included. Here, some additional finite element applications, using a fairly simple idealization, are presented in greater detail and comparisons of the results of the different independent analyses available so far are made, giving further evidence of the practical utility of Eshelby's method. New results on double-edge notched specimens are also included.

1. Introduction

A basic understanding of fundamental processes causing fracture in solids is the main theoretical aim of fracture mechanics but an important engineering requirement is the establishment of a continuum model providing calculable and measurable parameters which can characterize unambiguously such fracture events as the initiation of crack growth and the onset of unstable crack propagation under monotonically increasing quasi-static mode I loading or which can be used in quantitative or qualitative descriptions of Fatigue Crack Propagation (FTP) under various types and modes of loading.

The traditional Linear Elastic Fracture Mechanics (LEFM) parameters [2] such as Griffith's energy release rate G, equal to Rice's path independent integral J and also to the first component of Eshelby's energy momentum tensor, Irwin's mode I stress intensity factor K_I or the Crack Opening Displacement (COD) are uniquely interrelated; any one of them can be used to characterize fracture in this ideal, but practically nonexistent, linear elastic material. A more realistic model applicable to most engineering materials assumes that fracture is preceded by plastic flow or other irreversible processes in the crack tip region even in the case of brittle or quasi-brittle materials under Small Scale Yielding (SSY) conditions, since the infinite stress due to the singularity emerging from a LEFM analysis is not physically admissible. In addition, the present trend is to stipulate near the crack tip a "process zone" in which the constitutive relations obeyed by the bulk of the elastic-plastic material are not applicable and in which a number of latent fracture micromechanisms can become active [3]. In materials exhibiting some ductility the process zone is deeply imbedded in the plastic zone, i.e., the process zone size r_z appreciably smaller than the crack tip plastic zone size r_p. The inclusion of r_z in a continuum model provides some link with microstructural dimensions, e.g., grain size, inclusion spacing, etc., and the ratio $\rho = r_z/r_p$ can be very relevant to fracture behaviour [4,5,6].

Stress biaxiality in the crack tip region can affect the values of such quantities as r_p and ρ which play a significant role in fracture phenomena [7,8,9,10,11,12]. In addition, stress biaxiality can affect the fracture micromechanisms both qualitatively and quantitatively. For instance the hydrostatic component of the stress and the maximum tensile stress, which are related to the state of biaxiality, can influence the rates of void formation and growth in the process zone. Also, the dependence of directional stability of crack propagation on the state of stress biaxiality has been known for some time [13,14,15,16].

The stress and strain fields within the plastic enclave cannot be determined by using LEFM type analyses. However, under SSY conditions, using a boundary layer approach, it can be assumed that the crack tip plastic zone is contained in a mainly elastic circular region with the crack tip as its centre and radius R, where R is large compared to r_p. Nevertheless R can still be considered sufficiently small compared to the crack length or other structural dimensions for the stress and strain fields within the region to be adequately represented by LEFM parameters when the material is linear elastic. Hopefully, the tractions exerted by the elastic region forming the bulk of the specimen, on the periphery of the circular region containing the crack tip plastic and process zones and, in particular, the state of stress biaxiality, can be described satisfactorily by using appropriate terms of the elastic asymptotic solution, albeit that the latter does not take into account the presence of the crack tip plastic zone.

2.1. The *T*-term as a biaxiality parameter

For the reasons mentioned it is perhaps natural to define a LEFM biaxiality parameter to be used in conjunction with J, G or K_I. Such a parameter which has been suggested by a number of authors [17,18,19] is the elastic T-term, given by the first non-singular term in Williams' eigenfunction expansion [20]. Thus, for the Inglis configuration, namely that of a crack of length 2a in an infinite plane, loaded by remote hydrostatic tension σ, the T-term vanishes. For a remote tension σ_p applied normally to the crack and a remote lateral stress σ_Q, applied parallel to the crack, $T = (\sigma_Q - \sigma_P)$. However, for more general geometries encountered in real structures or in fracture specimens, the evaluation of T can present difficulties. Numerical methods have been more successful and one designed to solve directly for the vector of the Williams series coefficients has been described by Leevers and Radon [21]. Under SSY conditions, J is not affected by the T-term [9,18].

2.2. The normalised T-term

Greater generality, as well as independence from the influence of specimen geometry on K_I, is obtained by non-dimensionalising the stress T e.g., by normalising T with respect to the stress σ_0 $(= K_I(\pi a)^{-1/2})$. This stress will be recognised as the stress applied remotely on the Inglis configuration such as will produce a stress intensity factor equal to K_I at the crack tip. Using $K_I = E'J$, where $E' = E/(1 - \nu^2)$, E being the modulus of elasticity and ν is Poisson's ratio, σ_0 becomes

$$\sigma_0 = (E'J/\pi a)^{1/2}$$

Adopting the notation used by Leevers and Radon,

$$B = T/\sigma_0 = T(\pi a/E'J)^{1/2}. \tag{1}$$

3.1. Eshelby's theorem

An alternative method of obtaining the elastic T-term due to Eshelby [1] is based on the evaluation of certain J contour integrals along paths remote from the crack tip, thus

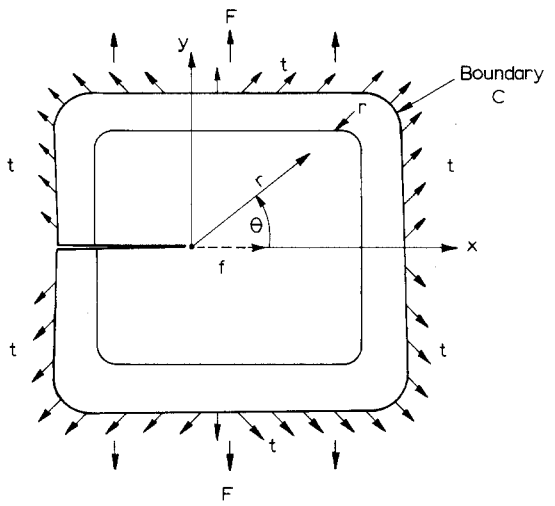

Figure 1. Cracked body subjected to external forces F. A point force f applied at the crack tip is resisted by tractions t.

circumventing the need for the seemingly more difficult task of establishing accurately the near tip fields (including the T-term). Hence for any specimen geometry the calculations can be carried out numerically using Finite Element Methods (FEM). A brief description of Eshelby's method follows.

Consider the cracked body shown in Fig. 1, in plane strain. External forces or tractions denoted by F are applied to the boundary and call the resulting stress, strain and displacement fields σ_{ij}, ϵ_{ij} and u_i, respectively. Next consider a semiinfinite crack in an infinite plane loaded by a point force f (per unit thickness) applied to the crack tip in a direction parallel to the crack, shown dotted on Fig. 1. This last configuration is a variant of Boussinesq's problem, for a point force applied to the apex of a wedge [22,23,24]. Using rectangular coordinates (x, y) or polar coordinates (r, θ), centered at the crack tip and using primes to denote the corresponding stress, strain and displacement fields σ'_{ij}, ϵ'_{ij} and u'_i, respectively, the analytical solution gives

$$\sigma'_{rr} = -f\cos\theta/(\pi r), \quad \sigma'_{\theta\theta} = \sigma'_{r\theta} = 0 \tag{2}$$

$$u'_1 = -(f/\pi E')\left[\ln(r/d) + y^2/\left(2r^2(1-\nu)\right)\right] \tag{3a}$$

$$u'_2 = -\left[f(1+\nu)/2\pi E\right]\left[(1-2\nu)\theta - xy/r^2\right] \tag{3b}$$

where d is the x-coordinate of a fixed point on the x-axis. (Note that (2) and (3) do not correspond to the physical situation when $f > 0$ since the y-displacements on the top crack face given by (3b) are negative when $\theta = \pi$.)

Now, if the plane region is not infinite but has some boundary C, the point force f must be resisted by tractions t applied to the boundary C, where t can assume any distribution of tractions provided that it is statistically equivalent to $-f$. In this case the stresses and the displacements within the region bounded by C will be given by (2) and (3) only if the tractions t are equal to $t_0 = \sigma'_{ij}n_j$ where n_j is the outward normal to the boundary C.

It will be recalled that the path independent integral J is given by

$$J = \int_\Gamma \left(W\delta_{ij} - \sigma_{ij}u_{i,1}\right)n_j \, ds \tag{4}$$

where W is the strain energy density, δ_{ij} are the Kronecker deltas, Γ is the path of integration and, here, n_j is the outward normal to Γ.

Let $J(F)$ denote the value of J when the specimen is loaded by the external forces F; let $J(f, t)$ denote the value of J when the point force f is applied at the crack tip and is resisted by the tractions t applied on the boundary C (which may conveniently coincide with the boundary of the specimen but not necessarily so). Finally let $J(F, f, t)$ give the J integral when the fields corresponding to F, f and t are superimposed; small displacement theory is assumed here.

The first form of Eshelby's theorem, which applies to the case when $t = t_0$, is given below:

$$J(F, f, t_0) = J(F) + Tf/E'. \tag{5}$$

When the point force f is resisted by tractions t which may differ from T_0, Eshelby's theorem takes the following second form:

$$J(F, f, t) = J(F) + J(f, t) + Tf/E' + 2K_I K_f/E' \tag{6}$$

where K_I is the stress intensity factor when the load F is applied on its own and K_f is the stress intensity factor included by the tractions $(t - t_0)$ applied on the boundary C on their own, i.e., without the point force f.

Now, by calculating J along circular paths of radius R surrounding the crack tip and shrinking R to zero, one is led to the expectation that if path independence is to be maintained the value of J can be different from zero only if the strain energy density singularity is of type r^{-1} [25]. But the fields due to the point force f resisted by t_0, given by (2) and (3) correspond to a strain energy density singularity of type r^{-2}, i.e., the stress and strain fields are 'too singular' for J to assume a non-zero value. Hence

$$J(f, t_0) = 0. \tag{7}$$

It is now apparent that when $t = t_0$ the second form given by (6) reverts to the first given by (5). (A proof of Eshelby's theorem is given in Appendix 1.)

4.1. Numerical evaluations of the *T*-term by Eshelby's method

It seemed a worthwhile exercise to examine whether acceptable working values of the non-dimensionalised T-term, B, could be obtained readily by FEM analyses, using relatively simple meshes. Figure 2 shows the different types of specimens analysed and their loading system. They include (a) the Single-Edged-Notched (SEN) specimen, (b) the Double-Edged-Notched (DEN) specimen, (c) the Centre-Cracked-Plate (CCP), (d) the Three-Point-Bend (BEND) specimen and (e) a simplified version of the Compact Tension Specimen (CTS), in which the load is applied at one end instead of the usual pin holes. In addition the Double-Cantilever-Beam (DCB) has essentially the same geometry as the simplified version of the CTS but has very small values of H/W ($= < 0.2$). The choice of specimens was governed by their general interest and frequent usage in fracture mechanics experiments but also on account of the possibility they afforded of comparisons with independent analyses, using different procedures or meshes, on similar specimens [17,21,1].

4.2. Finite element procedure

A typical finite element idealization is shown in Fig. 3a; the region near the crack tip is shown to a larger scale in Fig. 3b. Only the upper half, above the crack surface, is shown, taking advantage of the symmetry of the configurations. The mesh comprises 486 nodes and 442 "linear" isoparametric quadrilateral elements, with degrees of freedom vested in the nodal displacements u^n, v^n. The analyses were for plane strain. The modulus of elasticity was $E = 206840$ Mpa and Poisson's ratio ν was equal to 0.3.

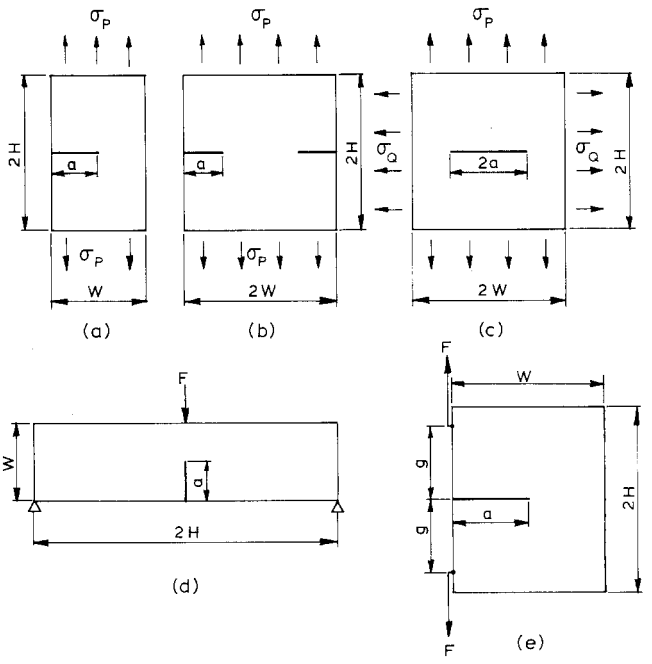

Figure 2. Specimen geometries: (a) Single-Edged Notch (SEN),(b) Double-Edged Notch (DEN), (c) Centre-Cracked-Plate (CCP), (d) Three-Point Bend (BEND), (e) A simplified version of a Compact Tension Specimen (CTS).

The first version of Eshelby's theorem was applied. First an attempt was made towards achieving a satisfactory representation of the stress field caused by the point force, given by (2). Using standard FEM procedure a routine was written to translate the tractions t_0 $(= \sigma'_{ij} n_j)$ into equivalent nodal forces applied on the external boundary nodes. The point force at the crack tip, f, was given the value of 2000 N (per unit thickness). Note however that the point force on the top half section of the specimen is only $f/2$. It also occurred that an improved representation of the crack tip fields could be obtained by "diffusing" the singularity caused by the point force. This was carried out by effectively suppressing the material in the small rectangle containing twelve elements, near the crack tip, shown in Fig. 3b, namely, by assigning to these elements a negligible thickness compared with unity. The point force f was then replaced by nodal forces, equivalent to the tractions t_0, applied to the near tip boundary nodes linking nodes 163, 166, 238 and 235, i.e., in a similar fashion to the equivalent nodal forces applied to the original more distant boundary.

Next the external forces F, alone, were applied on the external boundary nodes, using of course the complete mesh, including the twelve elements near the crack tip. Finally, the fields corresponding to (F, f, t_0) were obtained by superposition of the two preceding fields.

For the F loading, the usual boundary conditions were applied to the nodes on the x-axis (the axis of symmetry), namely, the crack tip node and those to its right were inhibited in the y-direction but were allowed to slide along the x-axis, with the possible exception of the last node to the right (node 469) which was fixed both ways when this was necessary to prevent rigid body translation, e.g., in the case of the SEN specimen. However, for the (f, t_0)-loading, a special feature of the stress field described by (2), is that the insertion of a crack along any radius emanating from the crack tip does not alter the stress field. This permitted the imposition of minimum boundary conditions consisting

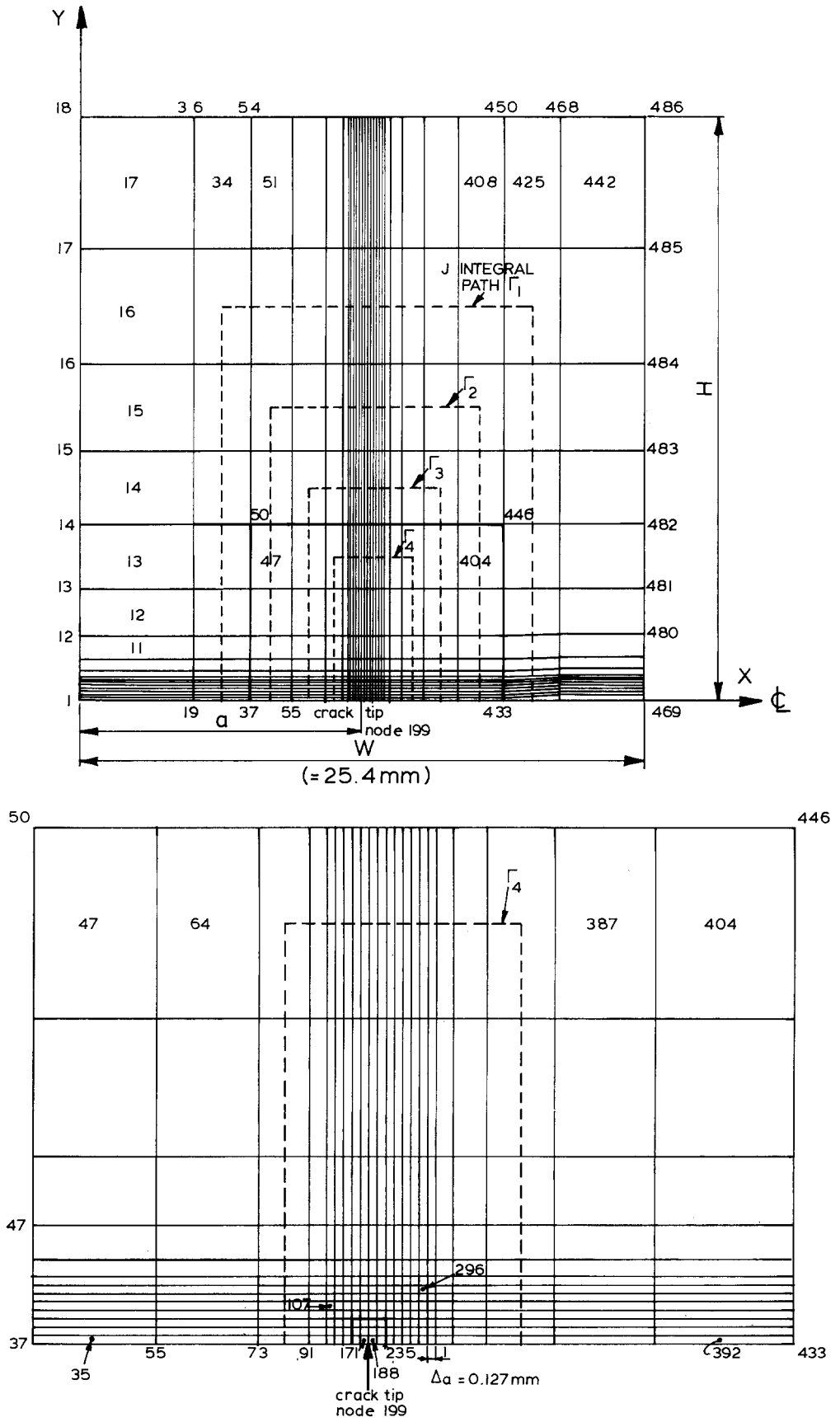

Figure 3. Typical finite element idealization (a) of half of the symmetrical specimen and (b) showing the region near the crack tip to a larger scale.

of the inhibition of node 235 (see Fig. 3b) in the y-direction and of node 469 both ways.

The J contour integrals were evaluated for the four progressively decreasing paths Γ_1, Γ_2, Γ_2 and Γ_4 shown in Fig. 3a.

4.3. Spot checks for the point force field

Some feel for the accuracy of the finite element representation of the stress field generated by the (f, t_0)-loading was acquired by a few spot check comparisons of the numerical values with the analytical values given by (2) and (3). Thus, to begin with, since the tractions t_0 imposed on the near tip and outside boundaries are, together, equivalent to a null field, the reactions at the inhibited nodes 235 and 469 must vanish and this was found to be true. Also, the vertical displacements of intervening nodes on the x-axis must be nil. The maximum value observed was less than 0.0007 mm, i.e., smaller than $0.0065u^{235}$, where u^{235} ($= 0.010939$ mm) is the horizontal displacement of node 235 when $a/W = 0.5$. The analytical value for the displacement at node 235, obtained with (3a) for $r/d = 0.02$, is 0.010957 mm. The FEM values of the displacements at the last node at the top right corner, with coordinates $r = 28.398$ mm, $\theta = 64.435$ are $u^{486} = -0.003719$ mm, $v^{486} = -0.000031$ mm, compared with the analytical values iu $= -0.003854$ mm and $v = -0.000086$ mm, respectively.

A spot check on the stresses is provided, for instance, by the stresses at the centre of element 107, situated in the region behind the crack tip, with coordinates $r = 0.80822$ mm, $\theta = 135°$. The numerical values of the principal stresses are $\sigma_1 = 555.1$ MPa, $\sigma_2 = -3.3$ MPa and $\phi = -44.4°$ compared with the analytical values $\sigma'_{rr} = 557.0$ MPa, $\sigma'_{\theta\theta} = 0$ and $\phi = -45°$ obtained by using (2). Here ϕ is the angle, measured in a counterclockwise sense, that the main principal stress makes with the x-axis. A second spot check at the centre of element 296 situated in the region ahead of the crack tip, with coordinates $r = 1.16743$ mm, $\theta = 45°$, gave $\sigma_1 = -385.2$ MPa, $\sigma_2 = 1.2$ MPa, $\phi = 45.1°$ for the FEM solution compared with $\sigma'_{rr} = -385.6$ MPa, $\sigma'_{\theta\theta} = 0$, $\phi = 45°$ for the analytical solution.

5.1. Results and discussion

Table 1 shows a typical output format summarizing the essential information emerging from the computer calculations for each case analysed. The top two lines give the type of specimen (SEN in the present case), its dimensions, the Load Factor (LF) for the applied load F and other information. The applied load F is equal to 6.8947 LF MPa in the case of an applied stress (or 100 LF N when F is a point load). Column 1 indicates the path of the J integrals. Columns 2, 3 and 4 give $J(F)$, $J(F, f, t_0)$ and $J(f, t_0)$, in N/mm, respectively. Column 5 gives the difference $J(F, f, t_0) - J(F) - J(f, t_0)$. Column 6 gives the value of T. Column 7 gives the nominal stress σ_0. Column 8 gives the geometric Y-Factor (YF), where $YF = \sigma_0/\sigma_P$ for the SEN, DEN and CCP specimens and σ_P is the normally applied stress (see Fig. 2). In the case of the point loads, F (per unit thickness), on the BEND and CTS specimens, YF indicates $(E'J)^{1/2}/K_0$ where $K_0 = 6M(\pi a)^{1/2}/W^2$. The nominal moment $M = FH/2$ for the BEND specimen and $M = FW$ for the CTS. Finally, column 9 gives the value of B obtained by using (1) and $J(F)$.

The absolute values of the figures for $J(f, t_0)$ in column 4 provide an additional indication of the adequacy of the numerical representation of the fields since according to (7) they should be nil. Generally, it was found that the more distant paths from the crack tip gave the more consistent results and only the first three were used in the final averaged results (A possible heuristic explanation is that whereas T does not depend on r, the stresses and the spurious numerical errors associated with them depend on $r^{-1/2}$ or r^{-1} and are therefore greater near the crack tip). However, exceptions were the DCB

Table 1. Typical computer output format giving breakdown of essential information in the calculation of the non-dimensional biaxiality term B

Path	$J(F)$	$J(F, f, t_0)$	$J(f, t_0)$	$J(F, f, t_0)$	T	s	YF	B
1	45.870036	44.544939	−0.000525	−1.324571	−150.535314	571.530346	2.072354	−0.263390
2	45.849760	44.510809	−0.001146	−1.337805	−152.039333	571.404015	2.071896	−0.266080
3	45.821463	44.492447	−0.005606	−1.323410	−150.403314	571.227663	2.071256	−0.263298
4	45.861950	44.620230	0.008710	−1.250430	−152.109272	571.479969	2.072171	−0.248669

Single-edged notched a = 10.160 mm, a/W = 0.4, H/W = 1.0, LF = 40.0, finemesh size = 0.127 mm, Poisson's ratio = 0.3, hor. fixed node = 469.

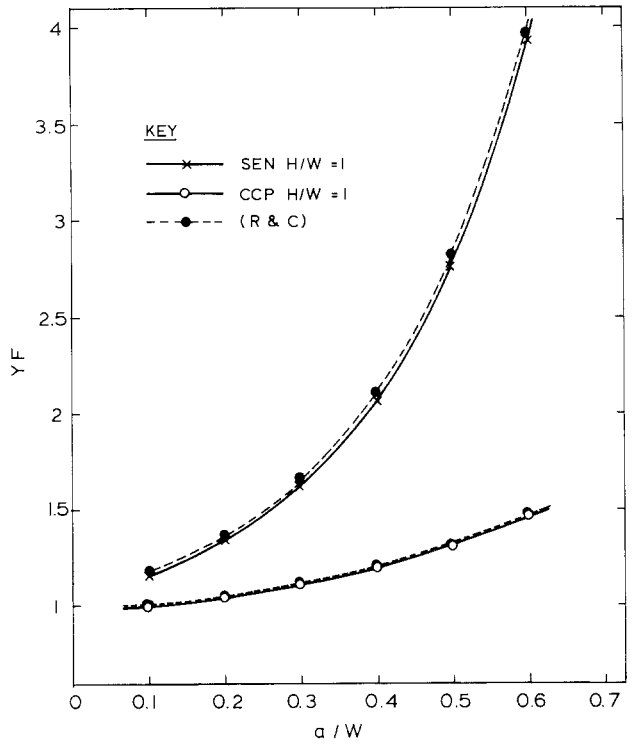

Figure 4. Geometric stress intensity Y-Factors (YF) for SEN and CCP specimens, derived from the integral $J(F)$, as functions of the non-dimensionalised crack length ratio a/W, compared with values of YF obtained from [26].

specimens for which the best results were obtained on Γ_4. Also, since the values of B appeared to be sensitive to the quality of the field description along the integration paths, only those paths were taken into account in the results for which the calculated values of $J(f, t_0)$ appearing in column 4 were numerically less than 0.006 N/mm.

Table 1 also shows, in passing, the path independence of the J integral. Thus, the values for $J(F)$ in column 2 vary by less than 0.12% while those for $J(F, f, t_0)$ in column 3 vary by less than 0.24%. In addition, a check on the geometric YFs is provided by column 8. Generally, these were found to be in good working agreement with the values obtainable from compendia such as Rook and Cartwright [26], as can be seen from Fig. 4 which presents comparisons of YF values for SEN and CCP specimens, showing good agreement. Another spot check comparison can be made for the normalised K_I value for the CTS specimen shown in Fig. 2e when $a/W = 0.5$. Thus, when the point load is at node 16, the value of $K_1 W^{1/2}/F$ is 9.48; cf. $Y = 9.60$ in [27].

Tests were also carried out with different values of the load factor LF and they showed, as expected, that the values of B did not depend on LF.

The results for the B values corresponding to the different specimen geometries are shown graphically in Figs. 5 to 8. An exception is made for the three DCB specimens for which a tabular representation (Table 2) is more appropriate.

Figure 5 gives the values of B against a/W for the SEN and DEN specimens. The comparison with L&R show close agreement in the case of the SEN specimen with $H/W = 0.5$ and also for the SEN with $H/W = 1$ and $a/W \geqslant 0.3$. Generally, the numerical methods encountered difficulties at the shorter crack lengths, $a/W \leqslant 0.1$. The only comparison available for the DEN specimens is the value of $B = -0.255$ for $H/W = 1$ and $a/W = 0.5$, given by Larsson and Carlsson (L&C), [17]; c.f. $B = -0.233$ in Fig. 5.

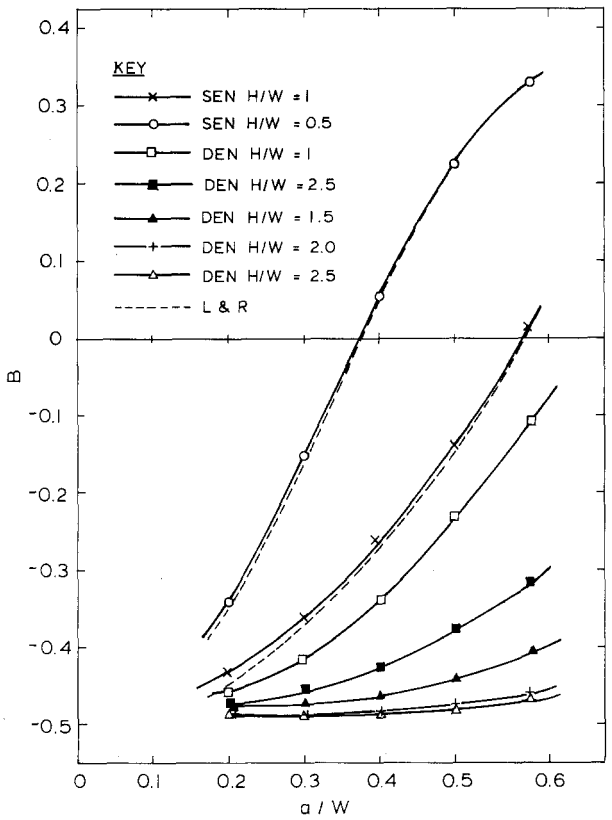

Figure 5. Values of the non-dimensional biaxiality parameter B for SEN and DEN specimens as functions of a/W and some comparisons with values obtained from [21].

The curves for the DEN specimens seem to indicate that, as H/W becomes large, the values of B do not depend on the ratio a/W and remain nearly constant at approximately -0.49.

Figure 6 gives the same type of results as the previous figure but for the CCP under uniaxial and equibiaxial loading. The biaxiality parameter $\lambda = \sigma_Q/\sigma_P$ is used. Again agreement with L&R is good. (Agreement between L&R and CGHK was close for the uniaxial loading mode, and also with the value obtained by Larsson and Carlsson, namely, $B = -1.044$, for $a/W = 0.5$.). It will be recalled that the limiting theoretical values of B, as a/W tends to zero are -1 and 0, for the uniaxial and equibiaxial cases, respectively.

Figure 7 covers the BEND and CTS specimens. The general agreement for the BEND specimen is less good than in the previous cases but it is still acceptable and they all follow the same trend. The results of the present analysis fall between L&R and CGHK. The value given by L&C for $H/W = 2$ and $a/W = 0.5$ is $B = 0.058$. The curves for the

Table 2. Comparisons of values of B obtained by independent analyses for the DCB specimens with $a/W = 0.5$, for different values of H/W

H/W	Present study	L&R	CGHK
0.05	7.513	6.364	7.399
0.10	4.842	4.783	4.795
0.20	2.956	2.942	2.829

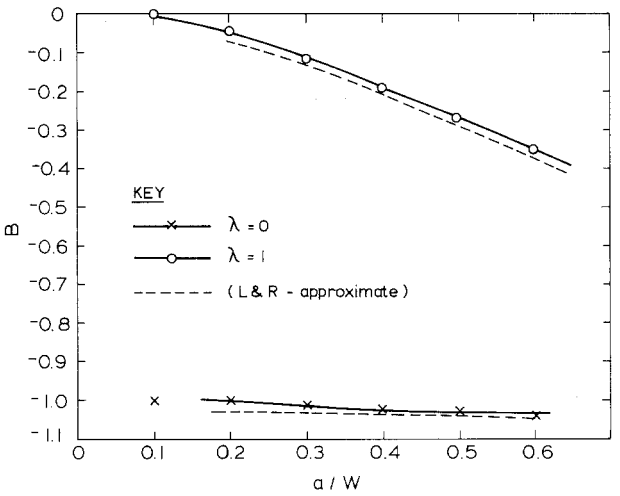

Figure 6. Values of B for CCP specimens under uniaxial and equibiaxial loadings, as functions of a/W, from the present study compared with values obtained from [21].

simplified version of the CTS do not provide a fair comparison at the smaller crack lengths in view of the difference in the geometries. Also, the value of B depends on the ratio g/H (see Fig. 2e) and the value of the ratio used in Fig. 5 was 0.8333. However, agreement with L&R is good when $a/W \geqslant 0.5$, i.e., for the geometries normally encountered in practice. The value given by L&C for the CTS with $a/W = 0.5$ is $B = 0.516$.

The results of the independent analyses on the DCB specimens for $a/W = 0.5$ are given in Table 2. Agreement between the different solutions seemed to deteriorate with decreasing values of the ratio H/W with the poorest for $H/W = 0.05$. The point of application of the end load (the distance g in Fig. 2e) had no bearing on the results for the three DCB specimens analysed.

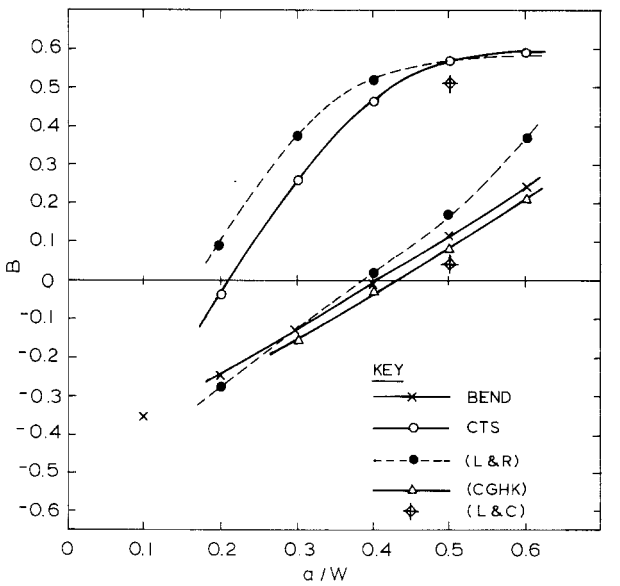

Figure 7. Values of B for the BEND specimens and for the simplified versions of the CTS as functions of a/W, and comparisons with values from [21], [1] and [17].

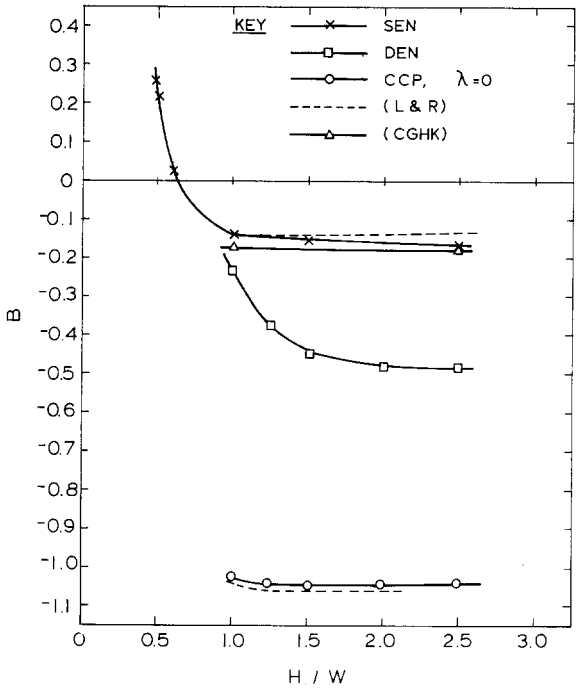

Figure 8. Values of B for the SEN, DEN and CCP specimens as functions of the ratio a/W, for a fixed crack length ratio $a/W = 0.5$, from the present study and, for the SEN and CCP, also from [21] and [1].

Figure 8 shows B for the SEN specimens and the CCP under uniaxial loading at the constant value $a/W = 0.5$, against H/W. Again agreement between the independent analyses is quite acceptable and the curves from the present analysis and L&R follow closely the same trend in the case of the CCP at the lower values of H/W (< 1.5). Values for the DEN specimens are also shown without comparisons.

Finally, the thought has occurred that, for the purpose of calculating the integral $J(F, f, t_0)$ using (4), the values of the (F, f, t_0)-fields could be obtained by superimposing on the FEM solution for the F-fields, the analytical solution for the (f, t_0)-fields obtained from (2) and (3), but this has not yet been tried. However, there may be some merit in obtaining all the fields by FEM since (5) and (6) involve differences and it is plausible that some of the inherent numerical discrepancies may cancel out in the process. Possible future tests may show.

6. Conclusion

Eshelby's theorem provides a simple and effective device for the calculation of the T-term by means of certain J contour integrals evaluated along paths at some distance from the crack tip and the method is well suited to elastic finite element types of analysis.

Consistent results, in good agreement with those from independent studies, have been obtained using comparatively simple meshes comprising "linear" isoparametric quadrilateral elements, provided certain precautions, described in the text, were taken.

Acknowledgement

The author wishes to thank Dr I.C. Howard for many useful discussions and to indicate the cooperative nature of the work on the development of Eshelby's method of evaluating the elastic T-term, which forms the main subject matter of this paper.

References

[1] G.E. Cardew, M.R. Goldthorpe, I.C. Howard and A.P. Kfouri, in *Fundamentals of Deformation and Fracture*, Proceedings of the Eshelby Memorial Symposium (ed.) B.A. Bilby, K.J. Miller and J.R. Willis, Sheffield 2–5 April 1984, Cambridge University Press (1985).

[2] J.R. Rice, in *Fracture, An Advanced Treatise*, Vol. II (ed.) H. Liebowitz, Academic Press (1968) 191–311.

[3] M.F. Ashby, C. Gandhi and D.M.R. Taplin, *Acta Metallurgica* 27 (1979) 699–729.

[4] A.P. Kfouri and J.R. Rice, *Fracture 77, Advances in Research on the Strength and Fracture of Materials*, D.M.R. Taplin (ed.) Vol. I, Pergamon Press (1978) 41–60.

[5] A.P. Kfouri and K.J. Miller, *Proceedings Institute of Mechanical Engineers* 190 (paper 48/76) (1976) 571–584.

[6] A.P. Kfouri, "On Double Limits and Asymptotic Small Scale Yielding Solutions of Crack Tip Fields", paper presented at the Symposium on Energy Release Rates and Path Independent Integrals in Defect and Fracture Mechanics, Bad Honnef, F.R.G., Jan 9–11, 1985.

[7] P.D. Hilton, *International Journal of Fracture* 9 (1973) 143–156.

[8] K.J. Miller and A.P. Kfouri, *International Journal of Fracture* 10 (1974) 393–404.

[9] A.P. Kfouri and K.J. Miller, *Fracture 77, Advances in Research on the Strength and Fracture of Materials*, D.M.R. Taplin (ed.) Vol. 3, Pergamon Press (1978) 241–246.

[10] K.J. Miller and A.P. Kfouri, in *ASTM STP 668* (1977) 214–228.

[11] J. Eftis, N. Subramonian and H. Liebowitz, *Engineering Fracture Mechanics* 9 (1977) 753–764.

[12] P.S. Theocaris and E. Gdoutos, *Engineering Fracture Mechanics* 7 (1975) 331–340.

[13] B. Cotterell, *International Journal of Fracture Mechanics* 2 (1966) 526–533.

[14] P.S. Leevers, J.C. Radon and L.E. Culver, *Journal of the Mechanics and Physics of Solids* 24 (1976) 381–395.

[15] H. Kitagawa and R. Yuuki, *Fracture 77, Advances in Research on the Strength and Fracture of Materials*, D.M.R. Taplin (ed.) 3, Pergamon Press (1978) 201–211.

[16] B. Cotterell and J.R. Rice, *International Journal of Fracture* 16 (1980) 155–169.

[17] S.G. Larsson and A.J. Carlsson, *Journal of the Mechanics and Physics of Solids* 21 (1973) 263–277.

[18] J.R. Rice, *Journal of the Mechanics and Physics of Solids* 22 (1974) 17–26.

[19] T.M. Edmunds and J.R. Willis, *Journal of the Mechanics and Physics of Solids* 25 (1977) 423–455.

[20] M.L. Williams, *Journal of Applied Mechanics* 24 (1957) 109–114.

[21] P.S. Leevers and J.C. Radon, *International Journal of Fracture* 19 (1982) 311–325.

[22] J. Boussinesq, *Application des Potentiels a l'Etude de l'Equilibre et du Mouvement des Solides Elastiques*, Gauthier-Villars, Paris (1885).

[23] J.H. Michell, *Proceedings London Mathematics Society* 32 (1900) 35.

[24] S.P. Timoshenko and Goodier, *Theory of Elasticity*, 3rd edition, McGraw-Hill, Inc. (1970).

[25] J.R. Rice and G.F. Rosengren, *Journal of the Mechanics and Physics of Solids* 16 (1968) 1–12.

[26] D.P. Rooke and D.J. Cartwright, *Compendium of Stress Intensity Factors*, H.M.S.O. (1976).

[27] K.J. Knott, *Fundamentals of Fracture Mechanics*, Butterworths (1973).

Appendix 1

Proof of Eshelby's theorem

The proof given here generally follows the line of [1]. Using the terminology and notation of the main text, from (4),

$$J(F, f, t_0) = \int_\Gamma \left[\tfrac{1}{2}(\sigma_{ik} + \sigma'_{ik})(\epsilon_{ik} + \epsilon'_{ik})\delta_{ij} - (\sigma_{ij} + \sigma'_{ij})(u_{i,1} + u'_{i,1}) \right] n_j \, ds \tag{A1}$$

$$J(F) = \int_\Gamma \left(\tfrac{1}{2}\sigma_{ik}\epsilon_{ik}\delta_{ij} - \sigma_{ij}u_{i,1} \right) n_j \, ds \tag{A2}$$

$$J(f, t_0) = \int_\Gamma \left(\tfrac{1}{2}\sigma'_{ik}\epsilon'_{ik}\delta_{ij} - \sigma'_{ij}u'_{i,1} \right) n_j \, ds = 0. \tag{A3}$$

The last equation in (A3) follows from (7) in the main text. Let

$$J_x = J(F, f, t_0) - J(F) - J(f, t_0). \tag{A4}$$

It is easily seen that J_x is associated with the 'cross terms' of the products in (A1),

$$J_x = \int_\Gamma \left[\tfrac{1}{2}(\sigma_{ik}\epsilon'_{ik} + \sigma'_{ik}\epsilon_{ik})\delta_{ij} - \sigma_{ij}u'_{i,1} - \sigma'_{ij}u_{i,1} \right] n_j \, ds. \tag{A5}$$

The stress strain relations for a linear material are $\sigma_{pq} = C_{pqrs}\epsilon_{rs}$, where C_{pqrs} are the elastic modulii. Hence,

$$C_{ikik} = \sigma_{ik}/\epsilon_{ik} = \sigma'_{ik}/\epsilon'_{ik}, \quad \text{or } \sigma_{ik}\epsilon'_{ik} = \sigma'_{ik}\epsilon_{ik} \tag{A6}$$

and

$$J_x = \int_\Gamma \left(\sigma'_{ik}\epsilon_{ik}\delta_{ij} - \sigma_{ij}u'_{i,1} - \sigma'_{ij}u_{i,1}\right) n_j \, ds. \tag{A7}$$

In the crack tip region,

$$\sigma_{ij} = K_I(2\pi r)^{-1/2}G_{ij}(\theta) + T\delta_{1i}\delta_{1j} + O(r^{1/2}) \tag{A8}$$

$$\sigma'_{ij} = fr^{-1}H_{ij}(\theta) \tag{A9}$$

where $G_{ij}(\theta)$ and $H_{ij}(\theta)$ are functions of the orientation angle θ. The only terms that contribute to J_x when the contour Γ is shrunk to the crack tip region is the cross term between T and f. This may be evaluated by considering a load involving only a laterally applied stress not contributing to the stress intensity K_I. Then,

$$\sigma_{ij} = T\delta_{1i}\delta_{1j}, \quad \epsilon_{11} = T/E'$$

$$\epsilon_{22} = -\nu(1+\nu)T/E, \quad \epsilon_{12} = 0.$$

Also,

$$u'_{1,1} = \sigma'_{11}/E' - \nu(1+\nu)\sigma'_{22}/E \tag{A11}$$

Substituting terms from (A10) and (A11) in the expression for J_x in (A7), after some manipulation and cancelling out of terms, we have

$$J_x = -\int_\Gamma \sigma'_{ij}n_j u_{i,1} \, ds = -(T/E')\int_\Gamma \sigma'_{ij}n_j \, ds.$$

But $\int_\Gamma \sigma'_{ij}n_j \, ds$ is the integral of the tractions t_0 which are statistically equivalent to $-f$, i.e.,

$$f = -\int_\Gamma \sigma'_{ij}n_j \, ds \tag{A12}$$

Hence

$$J_x = Tf/E' \tag{A13}$$

and

$$J(F, f, t_0) - J(F) = Tf/E'. \tag{A14}$$

To prove the second form of the theorem, given by (6), consider tractions t resisting the point force f applied to the crack tip, where $t \neq t_0$. Using the principle of superposition, the tractions t can be looked upon as the sum of two sets of tractions, namely, t_0 and $(t - t_0)$. Now σ'_{ij} will be given by

$$\sigma'_{ij} = fr^{-1}H_{ij}(\theta) + K_f(2\pi r)^{-1/2}G_{ij}(\theta) + T_f\delta_{1i}\delta_{1j} + \mathrm{O}(r^{1/2}) \tag{A15}$$

where K_f is the stress intensity factor induced at the crack tip by tractions $(t - t_0)$, on their own (i.e., without, of course, the point force f) and T_f is the T-term associated with the loading $(t - t_0)$.

Consider "external" forces $F_1 = (t - t_0)$ and apply the theorem by substituting F_1 for F in (A14),

$$J(F_1, f, t_0) = J(F_1) + T_f f/E'$$

or

$$J(f, t) = \left(K_f^2 + T_f f\right)/E'. \tag{A16}$$

Now apply the theorem again, this time using $F_2 = F + F_1$ as the "external" force,

$$J(F_2, f, t_0) = J(F_2) + T_2 f/E'$$

where $T_2 = T + T_f$ is the T-term corresponding to F_2, or

$$J(F, f, t) = J(F, F_1) + \left(T + T_f\right)f/E'$$

or

$$J(F, f, t) = \left[\left(K_I + K_f\right)^2 + \left(T + T_f\right)f\right]/E'.$$

Using (A16) this reduces to

$$J(F, f, t) = J(F) + J(f, t) + 2K_iK_f/E' + Tf/E'. \tag{A17}$$

When $t = t_0$, $F_1 = K_f = T_f = J(f, t) = 0$ and (A17) reverts to (14).

Résumé

On a proposé depuis un certain temps déjà, que le terme T élastique soit considéré comme un paramètre de biaxialité secondaire, à utiliser de concert avec le facteur d'intensité de contraintes KI, on l'intégrale J, en tant que paramètre primaire, pour caractériser les états de la rupture à l'extrémité d'une fissure. Lors d'une conférence récente, on a présenté un théorème, dû à Eshelby, qui fournit une méthode commode pour calculer le terme T, obtenue par une évaluation des intégrales de contour J appropriées. On a inclu des exemples d'applications analytiques, semianalytiques et numériques. Dans la présente étude, on donne avec de plus amples détails quelques applications complémentaires des éléments finis, en utilisant une idéalisation assez simple, et l'on compare les résultats de diverses analyses disponibles jusqu'ici, ce qui convainc de l'utilité pratique de la méthode d'Eshelby.

On inclut également des résultats nouveaux obtenus sur des éprouvettes à double entaille latérale.